materials

MDPI

Article

Destabilization and Ion Conductivity of Yttria-Stabilized Zirconia for Solid Oxide Electrolyte by Thermal Aging

Hwanseok Lee [1], Kanghee Jo [1], Min-sung Park [1], Taewoo Kim [2] and Heesoo Lee [1,*]

[1] School of Materials Science and Engineering, Pusan National University, Busan 46241, Korea
[2] System & Energy Division Material Technology Center, Korea Testing Laboratory, Seoul 08389, Korea
* Correspondence: heesoo@pusan.ac.kr

Abstract: The degradation behavior of yttria-stabilized zirconia by thermal aging was investigated in terms of phase transformation, local atomic structure, and electrical conductivity. The average grain size of 8YSZ was increased from 20.83 μm to 25.81 μm with increasing aging temperature. All 8YSZ samples degraded at different temperatures had a predominantly cubic structure. The (400) peak of 8YSZ deteriorated at 1300 and 1400 °C shifted to a high angle, and the peak of tetragonal was not indexed. For 8YSZ degraded at 1500 °C, the (400) peak shifted to a lower angle, and the peak of tetragonal was identified. Analysis of the local microstructure of aged 8YSZ using extended X-ray absorption fine structure showed that the intensity of the Zr-O peak gradually increased and that the intensity of the peak of cationic Zr decreased as the aging temperature increased. The changes in the peaks indicate that the oxygen vacancies were reduced and Y^{3+} ions escaped from the lattice, leading to the destabilization of 8YSZ. The activation energies of 8YSZ at 1300 °C and 1400 °C were derived to be 0.86 and 0.87 eV, respectively, and the activation energy of 8YSZ at 1500 °C increased significantly to 0.92 eV. With the thermal deterioration of 8YSZ, the cation (Y^{3+}) escaped from the lattice and the number of oxygen vacancies decreased, resulting in the formation of a tetragonal structure and high activation energy at 1500 °C.

Keywords: thermal aging; phase transformation; short-range ordering; oxygen vacancy; local atomic structure; ion conductivity

check for updates

Citation: Lee, H.; Jo, K.; Park, M.-s.; Kim, T.; Lee, H. Destabilization and Ion Conductivity of Yttria-Stabilized Zirconia for Solid Oxide Electrolyte by Thermal Aging. *Materials* **2022**, *15*, 6947. https://doi.org/10.3390/ma15196947

Academic Editors: Cécile Autret-Lambert and François Gervais

Received: 22 August 2022
Accepted: 27 September 2022
Published: 7 October 2022

Publisher's Note: MDPI stays neutral with regard to jurisdictional claims in published maps and institutional affiliations.

Copyright: © 2022 by the authors. Licensee MDPI, Basel, Switzerland. This article is an open access article distributed under the terms and conditions of the Creative Commons Attribution (CC BY) license (https://creativecommons.org/licenses/by/4.0/).

1. Introduction

Oxygen sensors that operate under harsh conditions have been extensively developed in recent years, and zirconia electrolytes are in the spotlight because of their high ionic conductivity and excellent reliability [1,2]. Zirconia electrolytes are exposed to hazardous chemicals and extreme temperatures depending on the operating environment and operate in such environments for several years [3]. Long-term exposure to high temperatures causes degradation of the solid electrolyte, and the degradation changes the conductivity, affecting the accuracy and stability of the sensor [4]. In addition, the solid oxide membrane (SOM) process, which is an environmentally friendly metal electrolysis process using zirconia-based electrolyte as an oxygen-conducting membrane, has been studied recently [5,6]. Thus, ensuring the stability of zirconia-based electrolytes at high temperatures is becoming more important.

The electrical properties and stability of zirconia-based electrolytes depend on the dopant type and concentration [7]. Zirconia is a polymorphic oxide that is monoclinic at room temperature and transforms to tetragonal and cubic phases at approximately 1443 and 2643 K, respectively [8]. The high-temperature phases have an important role in structural and oxygen ion conduction, and they can be stabilized at room temperature through the substitution of Zr^{4+} with rare earth or alkali earth cations [9]. The solid solution is formed as di- or tri-valent metal oxides are substituted for Zr^{4+} in zirconia. At that time, the vacancies of O^{2-}, which are necessary for the thermally activated conduction

process, were formed to maintain electrical neutrality. The conductivity increases because of concentration of oxygen vacancies increases with increasing dopant content. However, after the highest value is reached, conductivity begins to decrease regularly as the dopant content increases [10].

Zirconia-based electrolytes are stabilized by doping zirconia with binary oxides such as CaO, MgO, Sc_2O_3, and Y_2O_3. Among them, yttria-stabilized zirconia (YSZ) has high ionic conductivity at high temperatures and is the most widely studied as a zirconia solid electrolyte [11,12]. It is well known that the conductivity of YSZ decreases during aging at high temperatures (approximately 1000 °C). Moghdam et al. [13] reported that the precipitation of the tetragonal phase in a cubic matrix decreased the conductivity of YSZ. Kondoh et al. [14] suggested the oxygen ion vacancies $(V_O^{\cdot\cdot})$ around dopant cations (Y^{3+}) are trapped in the dopant cations owing to Columbic forces, that is, short-range ordering. In addition, it has been reported that the grain boundary resistance increases due to glassy phase segregation and $Y_2Zr_2O_7$ or $Y_4Zr_3O_{12}$ phase precipitation by the formation of oxygen vacancy complexes [15,16]. YSZ is deteriorated by various factors, as described above, resulting in a decrease in conductivity. Many studies on the degradation mechanism have been conducted at temperatures below 1000 °C, whereas studies of the aging behavior at high temperatures above 1200 °C are required.

We studied heat stress-induced degradation behavior of 8 mol% Y_2O_3 stabilized zirconia (8YSZ) at 1300, 1400, and 1500 °C in terms of phase transformation, local atomic structure, and conductivity. XRD analysis is performed to confirm the phase transformation induced by aging, and the change in the local atomic structure is analyzed by the extended X-ray absorption fine structure (EXAFS) measurements. The changes in the electrical conductivity and activation energy with aging are investigated using impedance spectroscopy.

2. Experimental

8YSZ (TZ-8Y, Tosoh Co., Tokyo, Japan) was uniaxially pressed at 3 ton/m^2 to produce 20 mm disk specimens. The green bodies were sintered at 1600 °C with a heating rate of 5 K/min and held at this temperature for 6 h. Sintered specimens were polished to a thickness of 1 mm and were heated in a tube furnace at 1300, 1400, and 1500 °C in atmospheric pressure in air for 100 h. The X-ray diffraction (XRD) patterns of the degraded specimens were collected at room temperature using a step scan procedure (2θ = 10–90°, step interval: 0.02°, Cu-Kα radiation, Rigaku Ultima-IV, Rigaku), and extended X-ray absorption fine structure (EXAFS) experiments were performed at the Zr K-edge using the EXAFS facility of the 10C wide-XAFS beamline in the Pohang Accelerator Laboratory (PLS-II, Pohang, Korea). The storage ring was operated at 3.0 GeV with an injection current of 350 mA. The sample surfaces were observed using field-emission scanning electron microscopy (FESEM, MIRA3, TESCAN). The grain size was determined from the SEM images based on ISO 13383—1 [17]. The grain size was defined as the diameter of the circumscribed circle from the image analysis. AC impedance measurements were performed with an Ivium-Stat (Ivium, Eindhoven, The Netherlands) instrument in the frequency range of 10^6 Hz to 10^{-2} Hz using an excitation voltage of 10 mV, at an operating temperature of 1000 °C, in air.

3. Results and Discussion

SEM images of 8YSZ aged at 1300, 1400, and 1500 °C for 100 h (hereinafter termed 1300 °C 8YSZ, 1400 °C 8YSZ, and 1500 °C 8YSZ) are shown in Figure 1. The grain size increased from 10.53 μm to 25.81 μm by thermal aging, and the average grain sizes for 10 grains of the 8YSZ specimen at 1300, 1400, and 1500 °C were 20.83, 22.17, and 25.81 μm, respectively. This shows that the grain size gradually increased according to the thermal aging.

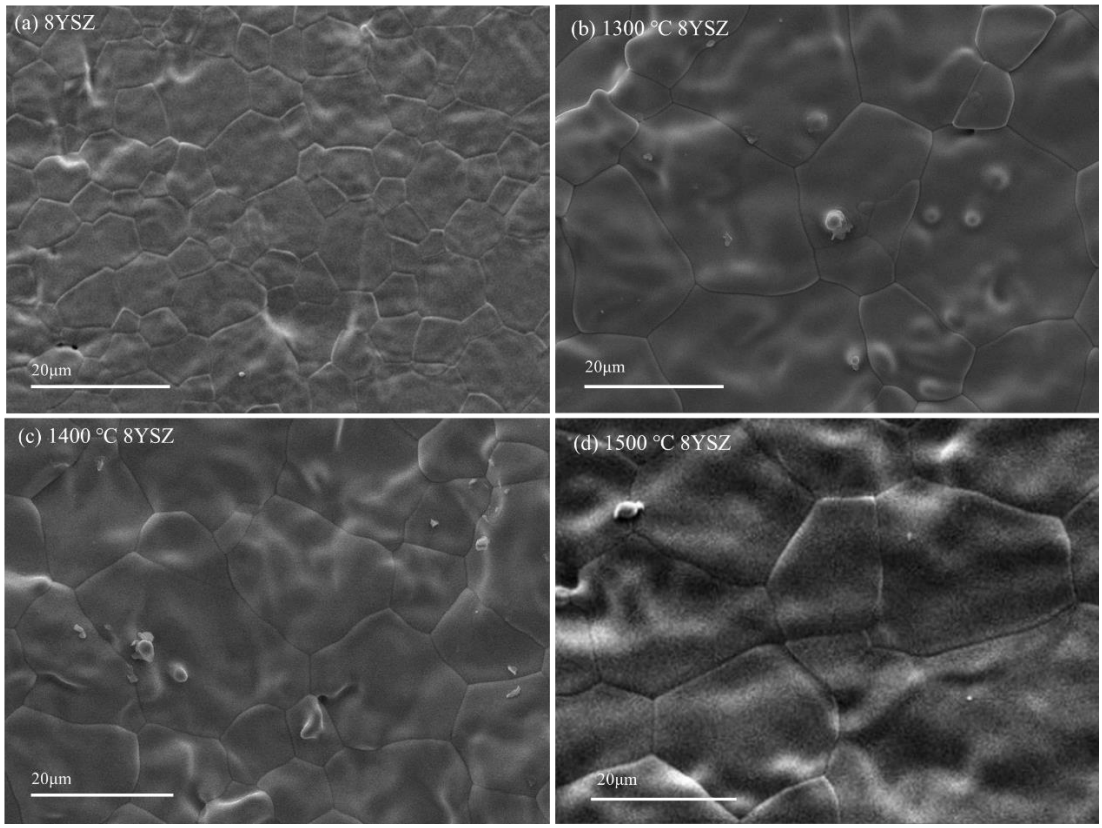

Figure 1. SEM images of specimens: (**a**) 8YSZ, (**b**) 1300 °C 8YSZ, (**c**) 1400 °C 8YSZ, (**d**) 1500 °C 8YSZ.

Figure 2 shows the XRD patterns of the aged 8YSZ. The (400) peak shifted to a higher angle for the 8YSZ specimens treated at 1300 °C and 1400 °C, and no new peak was observed. It was considered that lattice distortion due to the formation of a solid solution by the yttrium ions, which are larger than the zirconium ions, was relaxed by aging [18]. On the other hand, the peak shifted to a lower angle for the 1500 °C 8YSZ compared to 1300 °C and 1400 °C 8YSZ. It is related to the tetragonal peak observed at 1500 °C 8YSZ; the lower angle shift occurred with the formation of the tetragonal phase, which has a larger lattice [19].

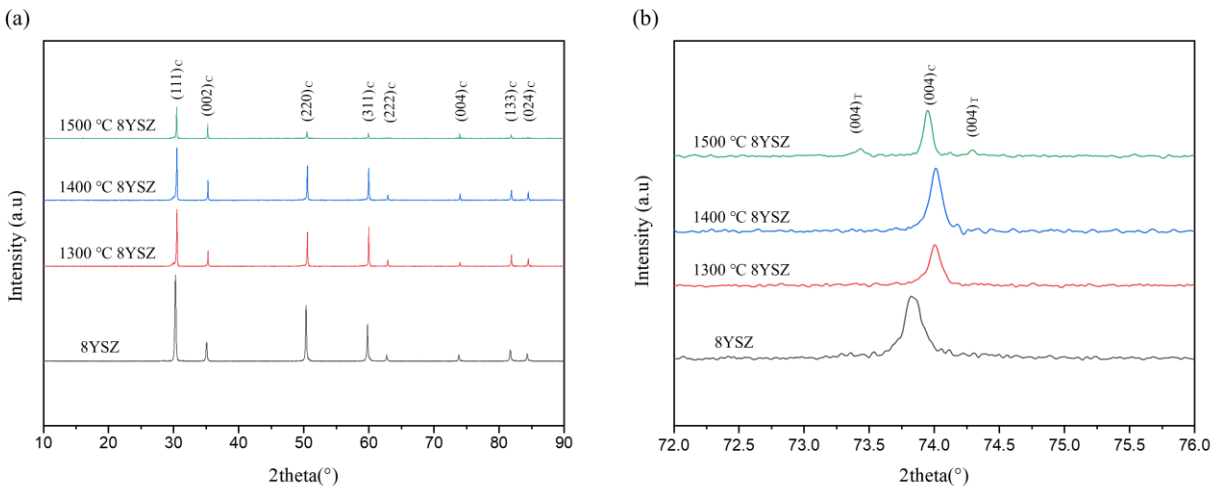

Figure 2. (**a**) XRD diffraction patterns and (**b**) (400) peaks of 8YSZ specimens after thermal aging for 100 h.

The Zr K-edge Fourier transform analysis using EXAFS was performed to confirm the degradation behavior according to thermal aging (Figure 3); EXAFS signals were obtained in the range of 3 < K < 11.5 Å using a Hanning window. The first peak at 1.7 Å is attributed to Zr-O bonding, and the second peak at 3.31 Å appeared with the Zr-Cation (Zr, Y) [20,21]. The interatomic distance from the Zr ion to the first nearest neighbor was decreased in 1300, 1400 °C 8YSZ by degradation. This suggests that the lattice distortion caused by the substitution of Y^{3+} ions is larger than that of Zr^{4+} ions and is relaxed by aging, resulting in short-range ordering of the oxygen vacancies [22]. However, for 1500 °C 8YSZ, the interatomic distance to the first nearest neighbor of Zr increased with the formation of the tetragonal phase. As the heat stress increased, the distance to the second nearest neighbor was shortened, the intensity of the Zr-Cation peak decreased, and the intensity of the Zr-O peak increased. These results mean that the number of oxygen vacancies decreased due to the formation of a disordered phase by extraction of the cation dopant (Y^{3+}). The increase in the intensity of the Zr-O peak for 1500 °C 8YSZ compared to that of 8YSZ treated at 1300 °C and 1400 °C corresponds to the previous XRD results [23].

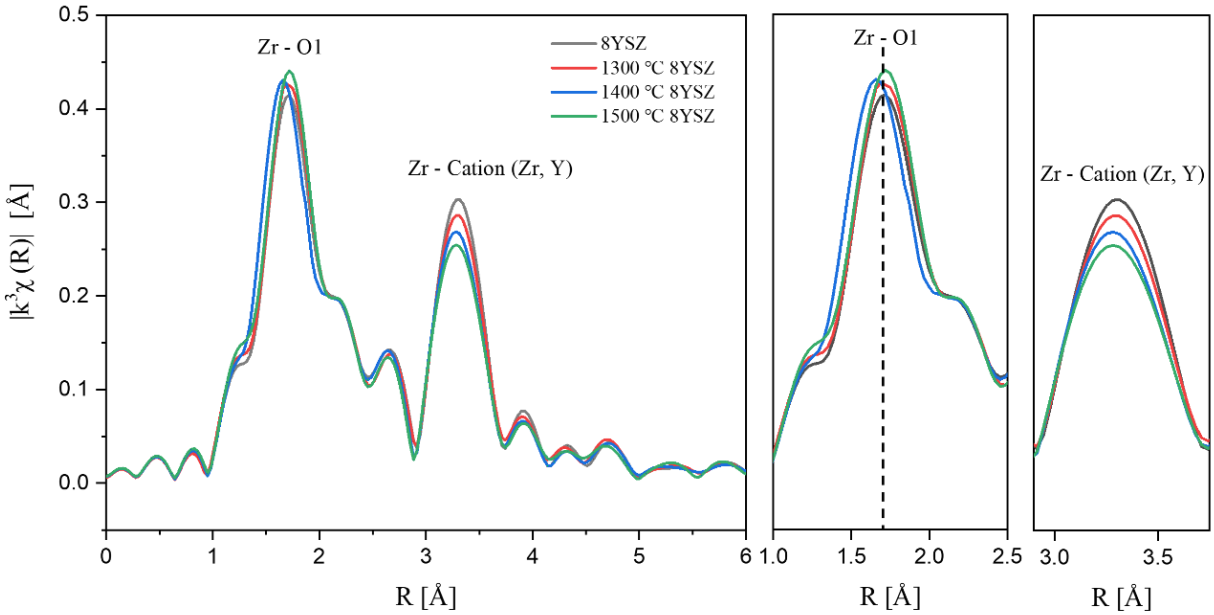

Figure 3. Zr K-edge Fourier-transform data for 8YSZ before and after thermal aging for 100 h.

Figure 4a shows the Nyquist plot from the impedance data for aged 8YSZ. The ohmic resistance (R_{ohm}) appeared in the intercept on the real axis in the high-frequency region, and the electrode polarization resistance (R_{pol}) was measured as the difference between the intercepts with the real axis at low and high frequencies [24]. R_{ohm} and R_{pol} increased as the heat stress increased, and the values of R_{pol} were 6.82, 8.81, and 18.25 Ω cm^2 for 8YSZ and the samples treated at 1300, 1400, and 1500 °C, respectively. The grain sizes increased with aging, but the area-specific resistance increased without decreasing. The increase in area-specific resistance by thermal degradation has a greater effect than the decrease in area-specific resistance due to the increase in grain size. Figure 4b shows the total ASR Arrhenius plots of 8YSZ before and after degradation. The activation energy of 1300 and 1400 °C 8YSZ was 0.86 and 0.87 eV, respectively, and the activation energy of 8YSZ at 1500 °C was significantly increased to 0.92 eV. It was considered that the short-range ordering hindered the diffusion of oxygen vacancies and increased the activation energy for 8YSZ treated at 1300 °C and 1400 °C, whereas for 1500 °C 8YSZ, the activation energy increased due to the formation of the tetragonal phase by Y^{3+} destabilization [25].

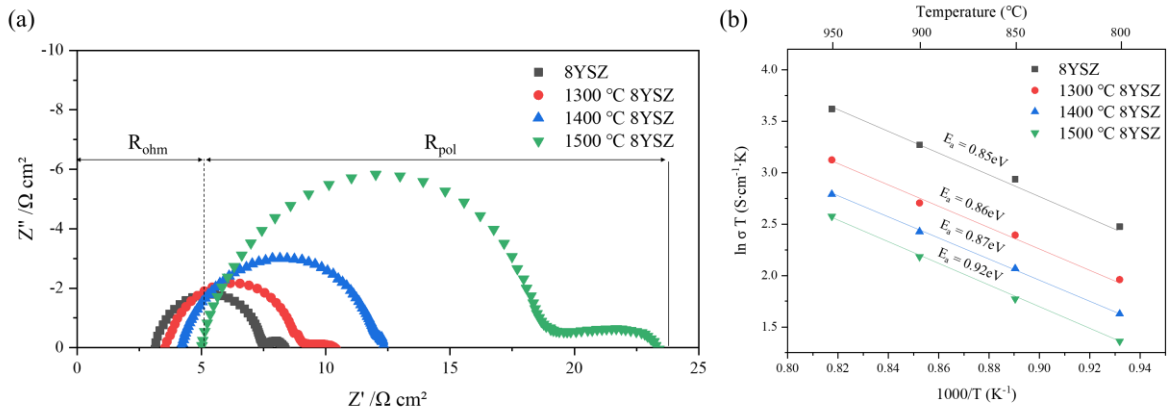

Figure 4. (**a**) Nyquist plot of 8YSZ before and after thermal aging; obtained in air at 1000 °C, (**b**) Arrhenius plots of the total ASR for 8YSZ before and after thermal aging.

4. Conclusions

We investigated the degradation behavior of yttria-stabilized zirconia by thermal aging in terms of phase transformation, local atomic structure, and electrical conductivity. The average grain size of 8YSZ aged for 100h at 1300–1500 °C increased from 20.83 µm (1300 °C) to 25.81 µm (1500 °C). The cubic phase was predominant in all aged 8YSZ, and a higher angle shift of the (400) peak occurred with thermal aging at 1300 °C and 1400 °C 8YSZ, where no peak of the tetragonal phase was observed. For 1500 °C 8YSZ, the peak shifted to a lower angle due to the formation of a tetragonal phase with a large lattice. Zr K-edge EXAFS analysis of the Zr-O local atomic structure showed that the intensity of the Zr-O peak increased, and the intensity of the Zr-Cation peak decreased as the aging temperature increased. This implies that oxygen vacancies were reduced and Y^{3+} ions escaped from the lattice, resulting in 8YSZ destabilization. The interatomic distance from the Zr ion to the first nearest neighbor was decreased in 1300, 1400 °C 8YSZ, which is related to the short-range ordering of oxygen vacancies. However, for 1500 °C 8YSZ, the interatomic distance to the first nearest neighbor of Zr increased with the formation of the tetragonal phase. The area-specific resistance measured by impedance spectroscopy was increased as the heat stress increased. The activation energy of 1300 and 1400 °C 8YSZ was 0.86 and 0.87 eV, respectively, and the activation energy of 8YSZ at 1500 °C was significantly increased to 0.92 eV. The difference in the activation energy of the specimens according to the deterioration conditions is attributed to the decrease in oxygen vacancies and the increase in lattice distortion with the formation of the tetragonal phase.

Author Contributions: Conceptualization, H.L. (Hwanseok Lee), K.J. and H.L. (Heesoo Lee); Formal analysis, H.L. (Hwanseok Lee), T.K.; Funding acquisition, H.L. (Heesoo Lee); Investigation, H.L. (Hwanseok Lee); Methodology, H.L. and M.-s.P.; Project administration, H.L. (Heesoo Lee); Resources, H.L. (Heesoo Lee); Writing—original draft, H.L. (Hwanseok Lee), K.J. and T.K. All authors have read and agreed to the published version of the manuscript.

Funding: This work was supported by a Korea Institute for Advancement of Technology (KIAT) grant funded by the Korean Government (MOTIE) (P0008335, The Competency Development Program for Industry specialist).

Institutional Review Board Statement: Not applicable.

Informed Consent Statement: Not applicable.

Conflicts of Interest: The authors declare no conflict of interest.

References

1. López-Gándara, C.; Ramos, F.M.; Cirera, A. YSZ-based oxygen sensors and the use of nanomaterials: A review from classical models to current trends. *J. Sens.* **2009**, *2009*, 258489. [CrossRef]
2. Badwal, S.P.S.; Foger, K. Solid oxide fuel cell electrolyte review. *Ceram. Int.* **1996**, *22*, 257–265. [CrossRef]

3. Shuk, P. Process Zirconia Oxygen Analyzer—State of Art Zirkondioxid-Sauerstoffsensoren—Stand der Technik. *TM. Tech. Mess.* **2010**, *77*, 19–23. [CrossRef]
4. Zhuiykov, S. *Electrochemistry of Zirconia Gas Sensors*; CRC Press: Boca Raton, FL, USA, 2007.
5. Milshtein, J.D.; Gratz, E.; Pati, S.; Powell, A.C.; Pal, U. Yttria stabilized zirconia membrane stability in molten fluoride fluxes for low-carbon magnesium production by the SOM process. *J. Min. Metall. Sect.* **2013**, *49*, 183–190. [CrossRef]
6. Hwang, K.J.; Shin, M.; Lee, M.H.; Lee, H.; Oh, M.Y.; Shin, T.H. Investigation on the phase stability of yttria-stabilized zirconia electrolytes for high-temperature electrochemical application. *Ceram. Int.* **2019**, *45*, 9462–9467. [CrossRef]
7. Liu, T.; Zhang, X.; Wang, X.; Yu, J.; Li, L. A review of zirconia-based solid electrolytes. *Ionics* **2016**, *22*, 2249–2262. [CrossRef]
8. Chervin, C.N.; Clapsaddle, B.J.; Chiu, H.W.; Gash, A.E.; Satcher, J.H.; Kauzlarich, S.M. Aerogel synthesis of yttria-stabilized zirconia by a non-alkoxide sol− gel route. *Chem. Mater.* **2005**, *17*, 3345–3351. [CrossRef]
9. Subbarao, E.C.; Maiti, H.S. Solid electrolytes with oxygen ion conduction. *Solid State Ion.* **1984**, *11*, 317–338. [CrossRef]
10. Weller, M.; Herzog, R.; Kilo, M.; Borchardt, G.; Weber, S.; Scherrer, S. Oxygen mobility in yttria-doped zirconia studied by internal friction, electrical conductivity and tracer diffusion experiments. *Solid State Ion.* **2004**, *175*, 409–413. [CrossRef]
11. Wu, C.J.; Hamada, M.S. *Experiments: Planning, Analysis, and Optimization*; John Wiley & Sons: New York, NY, USA, 2011.
12. Buzzi-Ferraris, G. Planning of experiments and kinetic analysis. *Catal. Today* **1999**, *52*, 125–132. [CrossRef]
13. Moghadam, F.K.; Stevenson, D.A. Influence of Annealing on the Electrical Conductivity of Polycrystalline ZrO_2 + 8 Wt% Y_2O_3. *J. Am. Ceram. Soc.* **1982**, *65*, 213–216. [CrossRef]
14. Kondoh, J.; Kawashima, T.; Kikuchi, S.; Tomii, Y.; Ito, Y. Effect of Aging on Yttria-Stabilized Zirconia: I. A Study of Its Electrochemical Properties. *J. Electrochem. Soc.* **1998**, *145*, 1527. [CrossRef]
15. Backhaus-Ricoult, M.; Badding, M.; Thibault, Y. Grain boundary segregation and conductivity in yttria-stabilized zirconia. In *Advances in Electronic and Electrochemical Ceramics: Proceedings of the 107th Annual Meeting of The American Ceramic Society*; Dongan, F., Kumta, P.N., Eds.; John Wiley & Sons: Baltimore, MD, USA, 2012; p. 173.
16. Navrotsky, A. Thermodynamics of solid electrolytes and related oxide ceramics based on the fluorite structure. *J. Mater. Chem.* **2010**, *20*, 10577–10587. [CrossRef]
17. International Standards Organization. *Fine Ceramics (Advanced Ceramics, Advanced Technical Ceramics)—Microstructural Characterization—Part 1: Determination of Grain Size and Size Distribution, ISO 13383-1*; International Standards Organization (ISO): Geneva, Switzerland, 2012.
18. Kondoh, J. Origin of the hump on the left shoulder of the X-ray diffraction peaks observed in Y_2O_3-fully and partially stabilized ZrO_2. *J. Alloy. Compd.* **2004**, *375*, 270–282. [CrossRef]
19. Kondoh, J.; Kikuchi, S.; Tomii, Y.; Ito, Y. Effect of Aging on Yttria-Stabilized Zirconia: II. A Study of the Effect of the Microstructure on Conductivity. *J. Electrochem. Soc.* **1998**, *145*, 1536. [CrossRef]
20. Dura, O.J.; Boada, R.; De La Torre, M.A.L.; Aquilanti, G.; Rivera-Calzada, A.; Leon, C.; Chaboy, J. XANES and EXAFS study of the local order in nanocrystalline yttria-stabilized zirconia. *Phys. Rev. B* **2013**, *87*, 174109. [CrossRef]
21. Khare, J.; Rajput, P.; Joshi, M.; Jha, S.; Bhattacharyya, D.; Kukreja, L. X-ray absorption spectroscopy based investigation of local structure in yttria stabilized zirconia nanoparticles generated by laser evaporation method: Effect of pulsed vs. CW mode of laser operation. *Ceram. Int.* **2015**, *41*, 5909–5915. [CrossRef]
22. Kondoh, J.; Kikuchi, S.; Tomii, Y.; Ito, Y. Effect of Aging on Yttria-Stabilized Zirconia: III. A Study of the Effect of Local Structures on Conductivity. *J. Electrochem. Soc.* **1998**, *145*, 1550. [CrossRef]
23. Ren, X.; Pan, W. Mechanical properties of high-temperature-degraded yttria-stabilized zirconia. *Acta Mater.* **2014**, *69*, 397–406. [CrossRef]
24. Appel, C.C.; Bonanos, N.; Horsewell, A.; Linderoth, S. Ageing behaviour of zirconia stabilised by yttria and manganese oxide. *J. Mater. Sci.* **2001**, *36*, 4493–4501. [CrossRef]
25. Kondoh, J.; Kikuchi, S.; Tomii, Y.; Ito, Y. Aging and composition dependence of electron diffraction patterns in Y_2O_3-stabilized ZrO_2: Relationship between crystal structure and conductivity. *Physica B* **1999**, *262*, 177–189. [CrossRef]